Electron transfer and near-field mechanisms in plasmonic gold-nanoparticle-modified TiO_2 photocatalytic systems

Electron Transfer and Near-Field Mechanisms in Plasmonic Gold-Nanoparticle-Modified TiO2 Photocatalytic Systems

Ramesh Asapu,[a] Nathalie Claes,[b] Radu-George Ciocarlan,[c] Matthias Minjauw,[d] Christophe Detavernier,[d] Pegie Cool,[c] Sara Bals,[b] and Sammy W. Verbruggen*[a]

[a] Dr. R. Asapu, and Prof. Dr. S.W. Verbruggen,* Department of Bioscience Engineering, Sustainable Energy Air & Water Technology, Campus Groenenborger, University of Antwerp, Groenenborgerlaan 171, Antwerp 2020, Belgium. *E-mail: Sammy.verbruggen@uantwerp.be

[b] Dr. N. Claes, Prof. Dr. S. Bals, Department of Physics, EMAT Research Group, Campus Groenenborger, University of Antwerp

[c] R-G. Ciocarlan, Prof. Dr. P. Cool, Department of Chemistry, LADCA Research Group, Campus Drie Eiken, University of Antwerp

[d] M. Minjauw, Prof. Dr. C. Detavernier, Department of Solid State Sciences, CoCooN Research Group, Ghent University, Krijgslaan 281/S1,Ghent 9000, Belgium

Abstract

The major mechanism responsible for plasmonic enhancement of titanium dioxide photocatalysis using gold nanoparticles is still under contention. This work introduces an experimental strategy to disentangle the significance of the charge transfer and near-field mechanisms in plasmonic photocatalysis. By controlling the thickness and conductive nature of a nanoparticle shell that acts as a spacer layer separating the plasmonic metal core from the TiO2 surface, field enhancement or charge transfer effects can be selectively repressed or evoked. Layer-by-layer and in situ polymerization methods are used to synthesize gold core–polymer shell nanoparticles with shell thickness control up to the sub-nanometer level. Detailed optical and electrical characterization supported by near-field simulation models corroborate the trends in photocatalytic activity of the different systems. This approach mainly points at an important contribution of the enhanced near field.

Introduction

The diverse application of plasmonic gold nanoparticles in multiple study fields such as photocatalysis(1−8) and sensing applications(9−12) has driven a tremendous amount of research. In the field of plasmon-enhanced photocatalysis, extensive research has been done with gold nanoparticles as it has been shown to improve the photocatalytic efficiency.(13−18) Although plasmonic gold-modified TiO2 photocatalytic systems are widely reported to have better performance than pristine TiO2 systems, the primary mechanism responsible for this enhancement is still under debate.(2,17,19−22) This study presents a novel approach to acquire new insights in the contributions from both the charge transfer (often also referred to as “hot electron”) and near-field enhancement mechanisms; the most frequently discussed theories related to plasmonic Au-TiO2 photocatalytic systems using small (<50 nm) nanoparticles. Different types of plasmonic Au-TiO2

photocatalytic systems were prepared using polyelectrolyte nanoparticle shells, acting as spacer layers, and compared with the pristine TiO2 reference. This was achieved by encapsulating the gold nanoparticles by either an insulating or conductive polymer shell that acts as a separating interface layer between the semiconductor photocatalyst surface and the plasmonic metal nanoparticle as shown in Figure 1. With a shell acting as either an insulating or conductive spacer layer, a clear distinction can be made between the charge transfer and near-field induced resonant energy transfer. Additionally, the spacer layer thickness can be fine-tuned by changing the polyelectrolyte shell thickness using established wet chemical methods. By increasing the shell thickness, the near field can be gradually suppressed. Thus, by keeping control over the shell thickness and its conductive properties, near-field enhancement and charge transfer effects can both be selectively repressed or evoked at the level of every single particle. This differs from the pioneering strategy applied by Awazu et al.,(23) who presented a related concept using silver nanoparticles fully embedded in an insulating SiO2 layer, separating them from the TiO2 film. A higher degree of control over the spacer layer thickness and its conductive properties, and by avoiding the blockage of active surface sites in our work (i.e., only very local contact between the shell and the TiO2 surface is established), is expected to result in a more exact and comprehensive experimental approach. Suppression of the near field was analyzed by finite element modeling (FEM) simulations using COMSOL Multiphysics and verified experimentally by surface-enhanced Raman spectroscopic (SERS) experiments. Additionally, SERS served as an experimental support to corroborate the near-field studies to find the distance dependency from the surface of the nanoparticle at which the near field is still active.

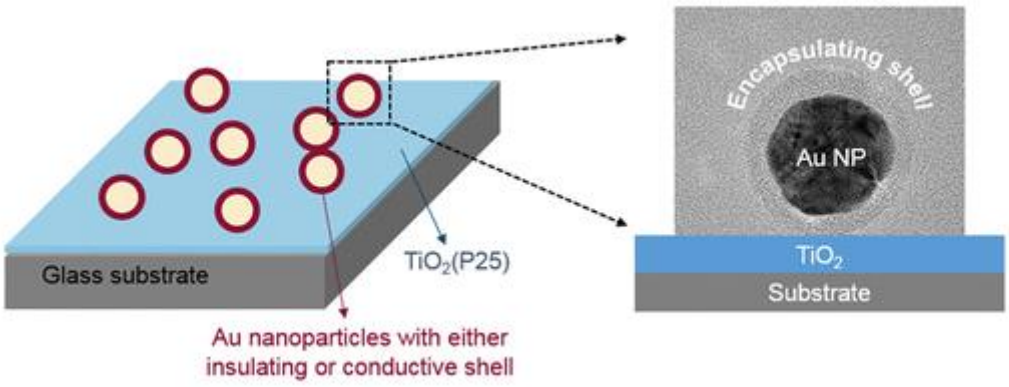

Figure 1. Design of Au-TiO2 plasmonic photocatalytic systems used in this work with TiO2 in contact with Au through an interfacial spacer layer.

Results and discussion

The different samples analyzed in this work are listed in Table 1 and consist of a pristine reference material and several Au-modified materials with both thin and thick, insulating and conductive spacer layers (i.e., shells). By comparing these composites and isolating the different effects, we aim to provide an improved understanding on how to make the best use of plasmonic nanostructures for enhancing TiO2 based photocatalytic systems. The insulating spacer layer between TiO2 and the gold

nanoparticle consists of a polyelectrolyte shell around the gold core prepared by the layer-by-layer (LbL) method.(24) On the other hand a conductive polyaniline (PANI) shell was synthesized by in situ polymerization of aniline around the gold core.(25)

sample description	spacer layer (shell) thickness, nm[a]	sample system/label
TiO_2, commercially available P25 (Evonik)		Ref_TiO_2
TiO_2 loaded with bare Au NPs	0	TiO_2 + Au
TiO_2 loaded with Au@polymer core@shell NPs (four layers), Au_L4, insulating shell/spacer layer	1.7 ± 0.5	TiO_2 + Au_L4
TiO_2 loaded with Au@polymer core@shell NPs (12 layers), Au_L12, insulating shell/spacer layer	3.2 ± 0.8	TiO_2 + Au_L12
TiO_2 loaded with Au@PANI core@shell NPs Au_PANI30, conductive shell/spacer layer	1.4 ± 0.5	TiO_2 + Au_PANI30
TiO_2 loaded with Au@PANI core@shell NPs Au_PANI90, conductive shell/spacer layer	4.1 ± 1.4	TiO_2 + Au_PANI90
TiO_2 loaded with Au@PANI core@shell NPs Au_PANI180, conductive shell/spacer layer	7.5 ± 1.6	TiO_2 + Au_PANI180

[a]As determined from TEM analysis.

Table 1. Different Samples of Pristine TiO2 and Au-TiO2 Systems Used for Photocatalytic Tests with Corresponding Labels

LbL Synthesis of Insulating Polymer Shell Encapsulating the Gold NPs

The deposition of alternatingly charged polyelectrolytes around the colloidal gold nanoparticles results in a red shift of the plasmon absorption band (Supporting Information Figure S1), which is a good indication of the growth of the shell thickness, as confirmed by transmission electron microscopy (TEM) in Figure 2. Shells of ca. 1.7, 2.1, and 3.2 nm were obtained after capping gold nanoparticles by four, eight, and 12 polyelectrolyte layers, respectively, with an average Au NP diameter of 17 nm (Figure S2). The Au core and polymer shell could only be visualized simultaneously in an accurate and reliable way due to optimization of the TEM grid support, as described in our recent work.(26)

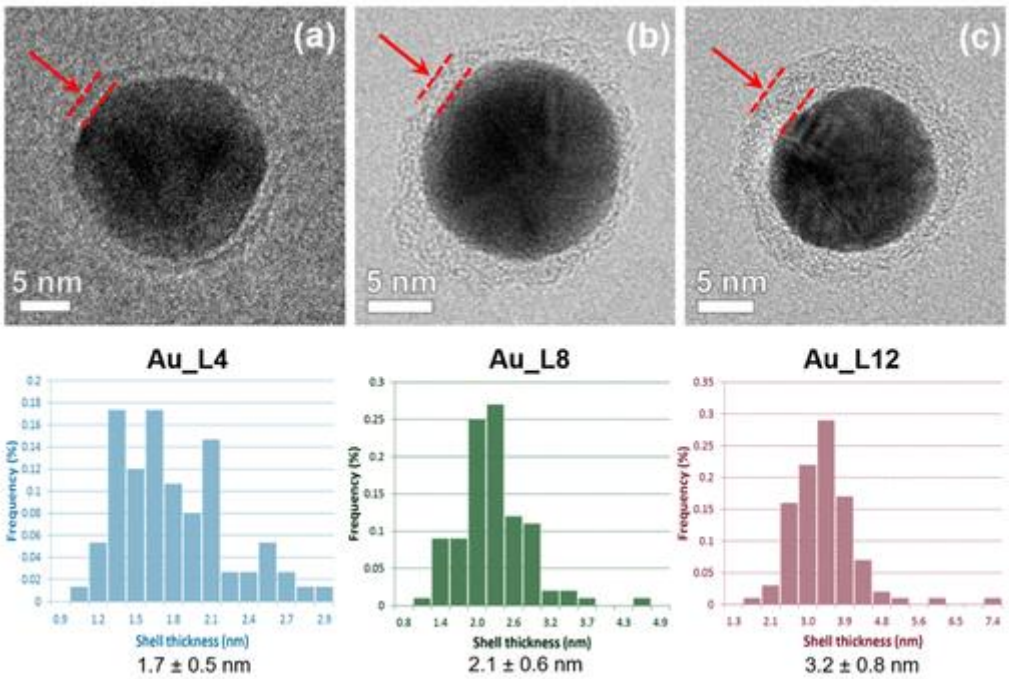

Figure 2. TEM images of Au@polymer core@shell nanoparticles and the corresponding mean shell thickness with the distribution for (a) four-layered (Au_L4), (b) eight-layered (Au_L8), and (c) 12-

layered (Au_L12) NPs. The shell thickness was determined by at least 100 measurements of multiple gold–polymer core–shell nanoparticles.

Synthesis of Conductive PANI Shell Encapsulating the Gold NPs

Au@PANI core@shell nanoparticles with a conductive shell were synthesized by in situ oxidative polymerization of aniline using acidic ammonium persulfate as the oxidant.(25) The UV–vis absorption spectra of aliquots removed after polymerization times of 30 (Au_PANI30), 90 (Au_PANI90), and 180 min (AU_PANI180) are shown in Figure S3a. The red shift in the SPR peak position (Figure S3b) is again evidence of the encapsulation of the gold core by a polyaniline shell. The shell thickness measurements were obtained by TEM analysis as shown in Figure 3. The increase in shell thickness is evident as the polymerization time is increased from 30 to 180 min. An ultrathin homogeneous PANI shell of thickness 1.4 nm is obtained for a polymerization time of 30 min (Figure 3a, Au_PANI30) that increases to 4.1 nm after 90 min (Figure 3b, Au_PANI90) and finally results in a thickness of 7.5 nm (Figure 3c, Au_PANI180) after 180 min of polymerization.

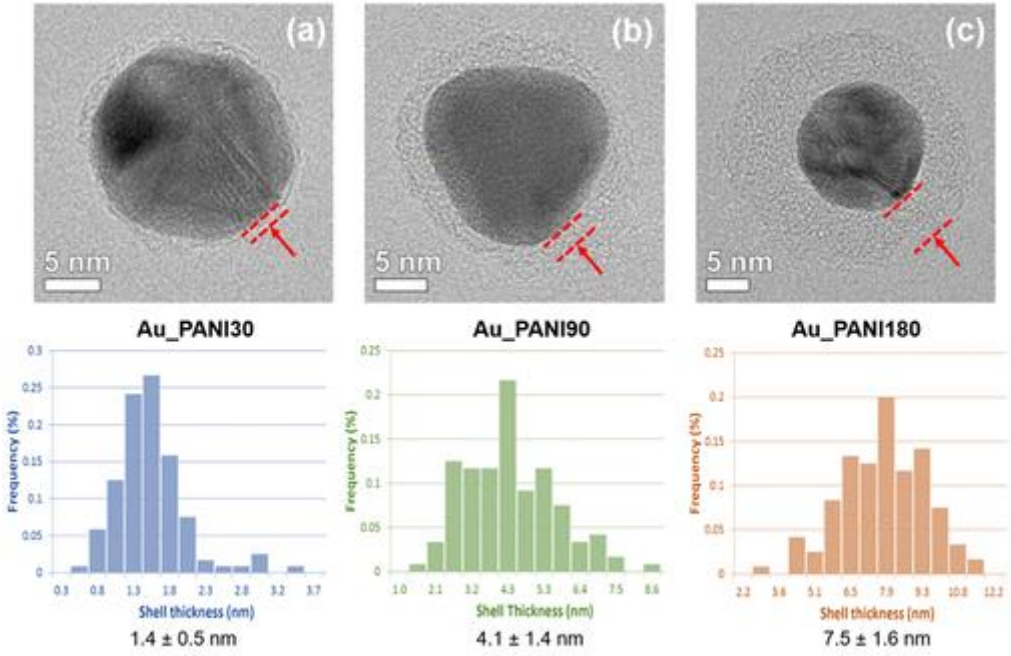

Figure 3. TEM images of Au@PANI core@shell nanoparticles and the corresponding shell thickness distribution for (a) 30 min (Au_PANI30), (b) 90 min (Au_PANI90), and (c) 180 min (Au_PANI180) of polymerization. The shell thickness was determined by at least 100 measurements of multiple gold–PANI core–shell nanoparticles.

Conductive Tip Atomic Force Microscopy Measurements

Experimental confirmation of the shell's electrical conductivity is of the utmost importance since the goal of the polyelectrolyte shell is to prevent hot electron transfer, while this should still be enabled with the PANI shell. The conductivity measurements were performed using conductive tip atomic force microscopy (C-AFM). Dilute colloidal solutions of gold–polymer core–shell nanoparticles were drop-casted on a substrate precoated with gold, in order to attain monolayer coverage and to evaluate the conductivity of the shell network in this drop-casted sample. From the C-AFM

measurements in Figure 4, it is clear that gold and gold@PANI nanoparticles are conductive in nature, whereas the four-layered (Au_L4) gold@polymer nanoparticles display typical behavior of an insulating material with high resistivity. This means that the polyelectrolyte shell of the core@shell sample Au_L4, composed of polymers (PAH/PSS)2 does not allow for electron or charge transfer through its medium. On the contrary, the similar core@shell structure of Au@PANI, i.e., sample Au_PANI180, exhibits good conductive properties. These results confirm that the polyelectrolyte shell effectively inhibits charge transfer and validates the conventional understanding that PANI is conductive. The latter is also supported by IV measurements (Supporting Information Figure S4), although a critical note should be added at this point that the minimal intrinsic electrical resistance of the thin PANI layers, which should be overcome by excited hot electrons for good conductivity, could not be quantified exactly. It is quite clear that the insulating Au@polymer core@shell NPs will rule out the role of the “hot electron” transfer effect, even for the thinnest shell thickness.

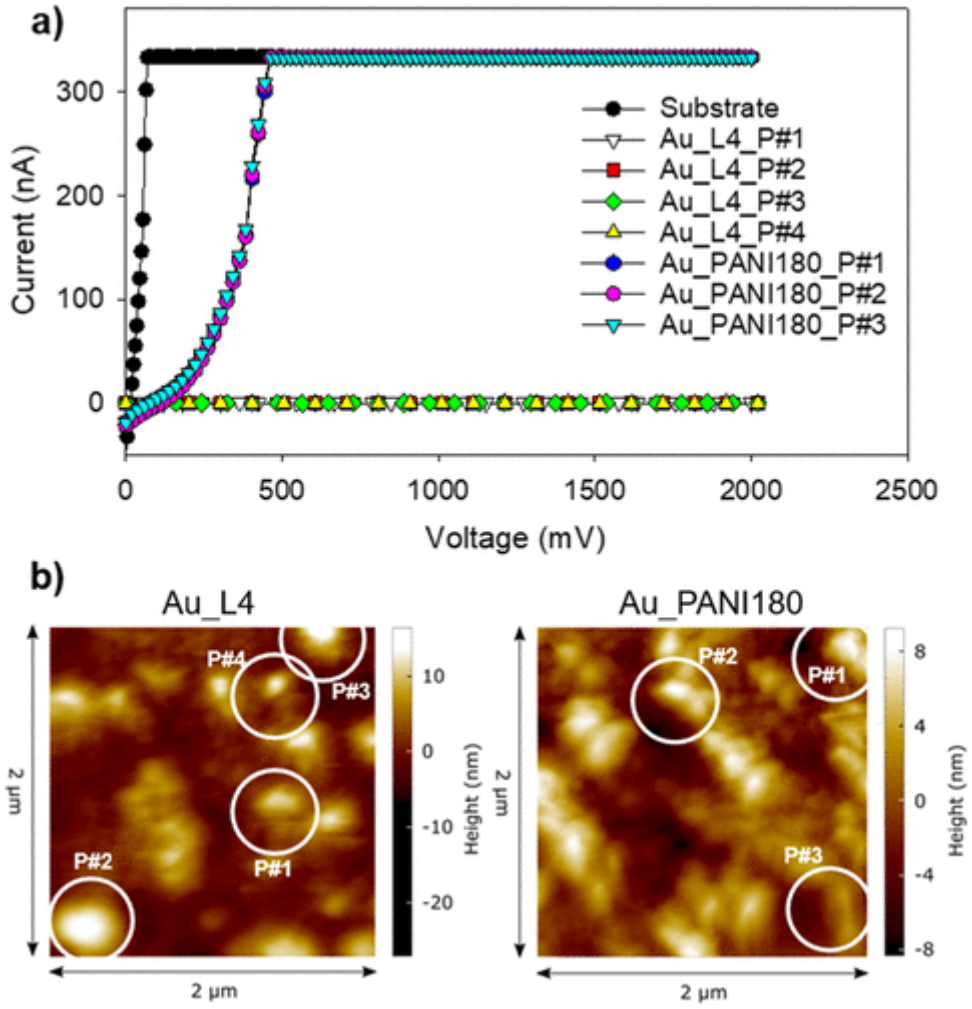

Figure 4. (a) Current–voltage (I–V) data performed on particles with corresponding numbers shown in AFM profile maps. (b) AFM surface profile maps of Au_L4 and Au_PANI180 nanoparticles drop-casted on gold-coated silicon substrate. The numbered particles on which the conductive-tipped AFM IV measurements were performed are shown in white circles.

Quantifying the Effect of Shell Thickness on Near-Field Properties Using SERS

For plasmonic nanomaterials such as gold nanoparticles, enhanced near fields are the main asset for plasmonic applications such as SERS. Therefore, it is important to study how the shell affects these near-field properties. For this specific purpose, SERS was used as an experimental tool to quantify the distance dependence of the near field from the surface of gold nanoparticles. In other words, by building polymer shells with high control over the shell thickness, the nanogap between adjacent gold cores can be tuned and the resulting hot spot effect can be regulated. The experimental SERS enhancement factors were corroborated with near-electric-field simulations and theoretically estimated SERS enhancement factors using COMSOL Multiphysics. So, in the next step, the Au@polymer core@shell NPs with increasing shell thickness lead to an increase in the distance between the NP metal cores and the surface, in turn leading to a gradually repressed near-field effect. The latter was verified by SERS measurements using a laser wavelength of 532 nm (Figure 5, red data plots), which corresponds best to the irradiation conditions employed during the photocatalytic tests (vide infra). The insulating property of the ultrathin polymer shell even rules out the charge transfer effect in SERS that sometimes comes into play depending on the selectivity of the probe molecule adsorption to the surface of the nanoparticles. The changes in the SERS enhancement in such systems can thus only be explained through changes in the near field. Consequently, the drop in the SERS enhancement factor (EF) with increasing interparticle distance is a direct result of decreasing electromagnetic field enhancement.

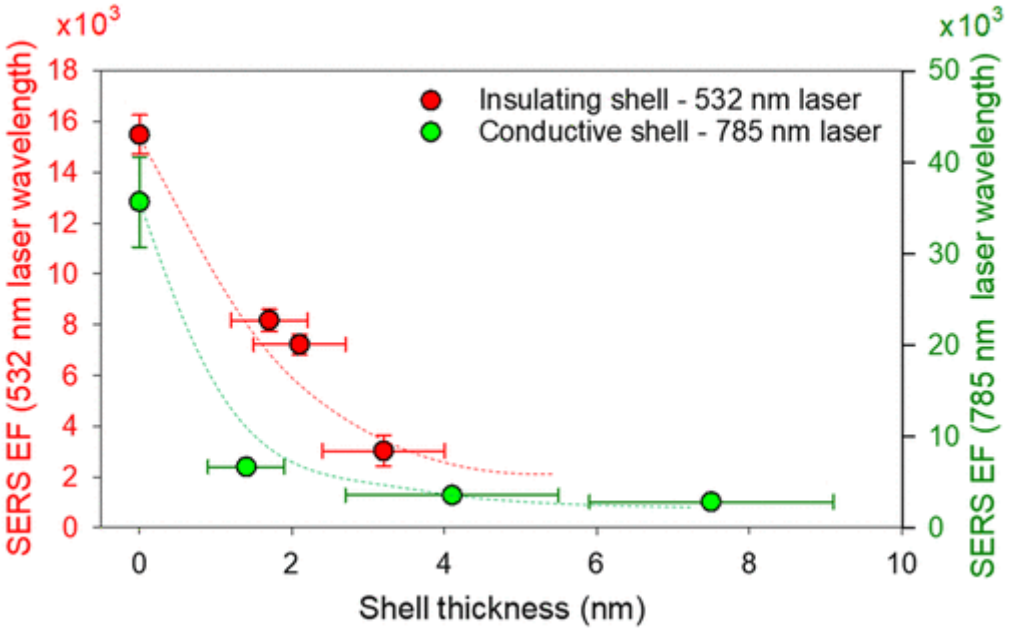

Figure 5. SERS enhancement factor calculated from the Raman spectroscopy measurements (Figures S6 and S7) as a function of nanogap between the gold nanoparticles. Error bars are the result of SERS measurements of n = 3 positions on the sample surface. Dotted lines provide easier visualization of the trend in EF decay as a function of shell thickness, which directly determines the nanogap.

This is also supported by the near-field simulations with the theoretical EF estimation(27) of (|E|/|E0|)4 performed in COMSOL Multiphysics as shown in Figure 6. The simulations assume that the Raman probe molecule (R6G) is present in the nanogap of a dimer NP system, which is a fair assumption since the NPs agglomerate when drop-casted on the SERS substrate (Figure S5), and are

validated in some of our previous studies.(28,29) The simulations show that the intense near-field interaction between two nanoparticles generates hot spots with decreasing intensity as the gap distance between two nanoparticle cores increases, as a result of the larger shell thickness. The comparison between the experimental and theoretical EF is shown in Figure S8. Additional SERS measurements were performed on NPs with conductive PANI shells (Figure 5, green data plots) at a laser wavelength of 785 nm to avoid the masking effect by the fluorescence displayed by PANI if the 532 nm laser would be used. These results also display the distance dependent decay of the SERS EF as a function of distance from the surface of the nanoparticle, i.e., nanogap distance in this particular set of experiments. Although some experimental variation may occur during the SERS sample preparation using LbL and PANI capped nanoparticles, it is clear that the overall EFs are of the same order of magnitude and the distance dependent EF decay is very similar for both systems. It should also not be overlooked that the bulk properties of samples may sometimes differ from the assumed dimer simulations in this study. However, the near-field simulations also corroborate the experimental results as observed from Figure S9. Moreover, the SERS experiments confirm the more important role played by the near field in hot spots compared to chemical enhancement.(27)

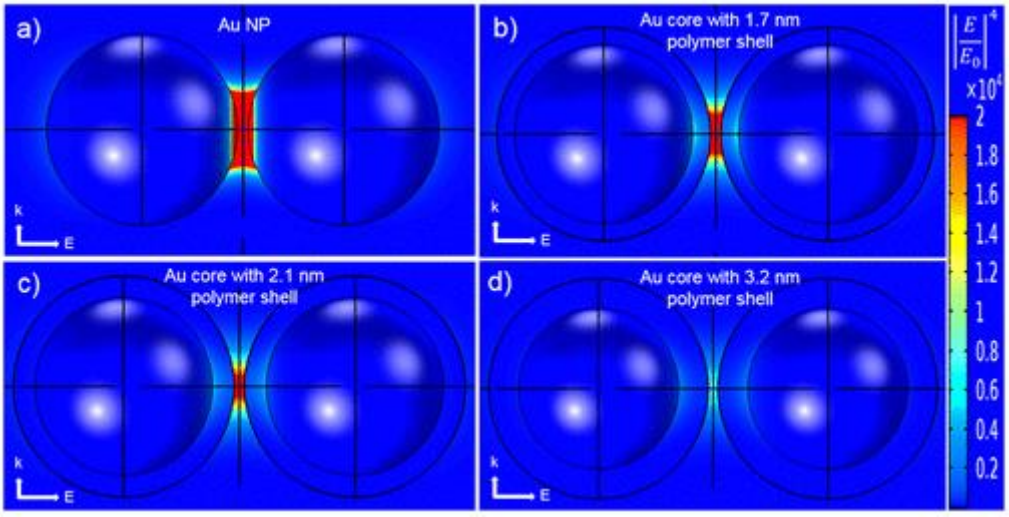

Figure 6. Near-field simulation maps at the Raman excitation wavelength of 532 nm in air for dimer systems of (a) Au nanoparticles and Au@polymer core@shell nanoparticles with a shell thickness of (b) 1.7 nm (Au_L4), (c) 2.1 nm (Au_L8), and (d) 3.2 nm (Au_L12) and a nanogap of 1 nm between the outer surfaces.

Photocatalytic Activity Measurements

As a reliable and reproducible photocatalytic test reaction, the degradation of a solid layer of stearic acid was measured under green LED light (λ = 515 nm, incident intensity of 15.3 mW/cm2; setup shown in Figure S10) according to the method by Paz et al.(30) Blank tests were performed to check the degradation effect of light and activity of pure gold nanoparticles in the absence of TiO2, which did not show any stearic acid degradation. It is also important to note that the PANI did not induce any sensitization effect under the present irradiation conditions. The results from the stearic acid degradation for all different Au-TiO2 photocatalytic systems listed in Table 1 are plotted in Figure 7. Since it is well-known that stearic acid degradation follows a zero order kinetic reaction in the case of flat and dense films,(31,32) linear regression fits for the degradation with the corresponding R2

values are also shown in Figure S11. The reaction rates given in Figure 7 provide a clear picture on the differences in photocatalytic activity between the samples. First, it is interesting to observe the visible light activity of the reference TiO2 sample (Ref_TiO2, i.e., P25, Evonik), which is rather unexpected given its band gap of 3.15 eV. However, it has been reported that P25, which consists of a 80–20 ratio of anatase–rutile phase crystals, shows reasonable visible light activity because of defects at the anatase–rutile interface.(33) Some researchers also demonstrated the visible light response by means of EPR and photoluminescence measurements of P25.(34,35)

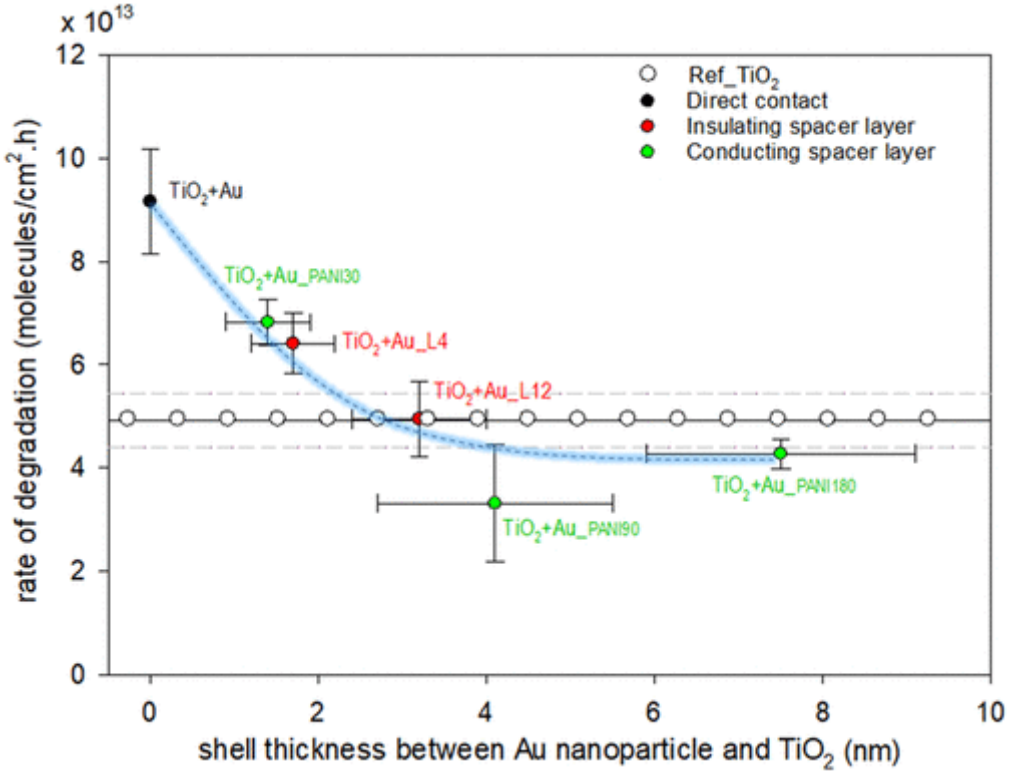

Figure 7. Rate of photocatalytic degradation of stearic acid by different Au-TiO2 systems under visible light (λ = 515 nm). The dotted line represents the trend of the distance dependent nature of different Au-TiO2 plasmonic photocatalytic systems. The gray dotted lines represent the error range for the TiO2 reference system.

The highest rate is obtained when bare gold nanoparticles are in direct contact with TiO2 (sample TiO2 + Au), which could be assigned to a synergetic effect of both direct hot electron transfer and near-electric-field enhancement. These processes boost the activity by increasing the rate of charge carrier formation resulting in enhanced stearic acid degradation compared to the reference system. When TiO2 is loaded with gold nanoparticles encapsulated with an ultrathin insulating polymer shell thickness of 1.7 and 3.2 nm, respectively (samples TiO2 + Au_L4 and TiO2 + Au_L12), the ultrathin polymer layer acts as an insulating spacer layer. In this scenario, direct electron transfer is no longer possible and the enhancement in the reaction rate (Figure 7, red data plots) can only be attributed to the near field at the active sites on the surface of TiO2 that contain defects.(2,17,36) An increase in the insulating spacer layer thickness, i.e., distance between TiO2 and Au nanoparticle, reduces the near-field intensity available at the surface of TiO2 resulting in the drop in photocatalytic reaction

rate enhancement (red data plots). The trend of decreased activity by gradually repressing the near field is confirmed by the simulation maps as seen from Figure 8a–c. This drop in the near field was furthermore corroborated with experimental evidence using SERS (Figures 5 and 6). The results indicate that at a gap of around 3 nm the field effects become insignificant as they no longer lead to improved photocatalytic activity as evidenced by the photocatalytic activity of sample TiO2 + Au_L12 (Figure 7), which shows no enhancement compared to the reference system. The sample with a thin conductive spacer layer (TiO2 + Au_PANI30) shows a significant improvement in the stearic acid degradation rate compared to the TiO2 reference system. In this case direct electron transfer from the excited gold nanoparticle into the TiO2 conduction band through the PANI spacer layer thickness, i.e., distance between TiO2 and Au nanoparticle, reduces the near-field intensity available at the surface of TiO2 resulting in the drop in photocatalytic reaction rate enhancement (red data plots). The trend of decreased activity by gradually repressing the near field is confirmed by the simulation maps as seen from Figure 8a–c. This drop in the near field was furthermore corroborated with experimental evidence using SERS (Figures 5 and 6). The results indicate that at a gap of around 3 nm the field effects become insignificant as they no longer lead to improved photocatalytic activity as evidenced by the photocatalytic activity of sample TiO2 + Au_L12 (Figure 7), which shows no enhancement compared to the reference system. The sample with a thin conductive spacer layer (TiO2 + Au_PANI30) shows a significant improvement in the stearic acid degradation rate compared to the TiO2 reference system. In this case direct electron transfer from the excited gold nanoparticle into the TiO2 conduction band through the PANI spacer layer is again enabled. In addition, the spacer layer thickness is only 1.4 nm, which is similar to the insulating spacer layer thickness of sample TiO2 + Au_L4, resulting in a similar near field available at the TiO2 surface (Figure 8b,d). Therefore, the near-field and direct electron transfer can concur in the TiO2 + Au_PANI30 system. It is interesting to note, however, that the improvement in the rate is not significantly higher than for the TiO2 + u_L4 sample, although hot electron transfer through the thin conductive shell is now enabled. On the contrary, the samples with a conductive PANI spacer layer follow exactly the same trend as those with insulating spacer layers, which is fully governed by the near-field-enhancement mechanism. The significant role played by the near field also confirms the findings from the systematic study by Awazu et al.(23) When the conductive spacer layer thickness is further increased to 4.1 and 7.5 nm (samples TiO2 + Au_PANI90 and TiO2 + Au_PANI180, respectively), there is no improvement in the rate and a decrease in the photocatalytic activity is observed from Figure 7 (green data plots). At these shell thicknesses, there is no significant electric field enhancement left as corroborated by both SERS studies (Figure 5) and near-field simulations (Figure 8e,f), although electron transfer is technically still possible. However, with no improvement in the photocatalytic reaction rate compared to the reference system, it seems the role of the direct electron transfer mechanism in the absence of near-field effects is rather limited. Additionally, a critical note should be added that the charge transfer process is of course also dependent on coupling of electronic states between Au and PANI at the interface and the electron transport characteristics of PANI, which are not accounted for in this study.(37)

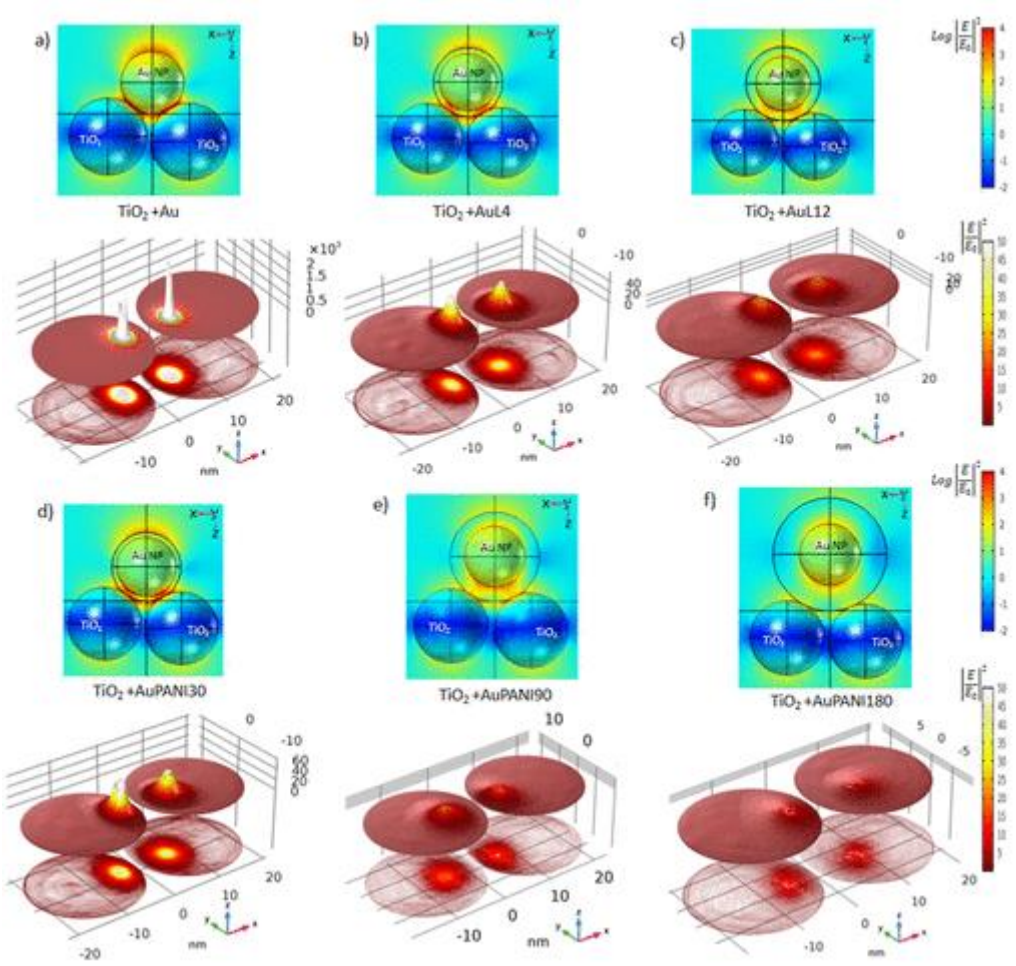

Figure 8. Field enhancement distribution maps of Au-TiO2 systems with the projection of TiO2 surface contours with a height intensity scale at the bottom of corresponding distribution maps for different systems (Table 1). Systems (a) TiO2 + Au, (b) TiO2 + AuL4, (c) TiO2 + AuL12, (d) TiO2 + AuPANI30, (e) TiO2 + AuPANI90, and (f) TiO2 + AuPANI180 represent the idea of a gold nanoparticle on top of two TiO2 nanoparticles. The field enhancement distribution maps are shown with a common logarithmic scale, and the TiO2 surface contours are shown with normal scale for better visualization.

Conclusion

An experimental approach is presented to systematically study the contribution of direct electron transfer and near-field enhancement in plasmonic photocatalysis. By the introduction of a nanoparticle shell acting as a spacer layer between the gold nanoparticle and the TiO2 surface, the importance of each mechanism could be studied by controlling the shell properties (thickness and conductive nature). It is shown, through a combination of theoretical simulations, SERS experiments, and photocatalytic activity tests, that for both insulating and conductive shells the near-field effect becomes insignificant for shell thicknesses exceeding 3 nm. Strikingly, conductive shells that enable electron transfer did not lead to a significant improvement in photocatalytic activity compared to systems prepared with insulating shells of a similar thickness. This observation hints at a dominant role of the near-field enhancement mechanism.

Methods

Synthesis of Au@polymer and Au@PANI Core@Shell Nanoparticles

Polymer-encapsulated gold nanoparticles were synthesized using the layer-by-layer method as described in literature.(24) The LbL process was continued until 12 layers of polyelectrolytes were encapsulating the gold core nanoparticle. The aliquots are labeled as per the corresponding layer number for convenience, i.e., Au_LX, where X is the number of layers. Polyaniline-encapsulated gold core–shell nanoparticles were synthesized by in situ polymerization of aniline at the surface of bare gold nanoparticles using the method described in literature.(25) The three aliquots are labeled as Au_PANI30, Au_PANI90, and Au_PANI180 for the samples with polymerization times of 30, 90, and 180 min respectively. Detailed synthesis procedure is provided in Supporting Information.

Photocatalytic Activity Tests

A 50 µL aliquot of 1 wt % ethanolic suspension of commercial TiO2 (P25, Aeroxide) was drop-casted onto six silicon wafers (precleaned by ultrasonication in methanol), so 0.5 mg of photocatalyst is present on each silicon wafer, and dried overnight at 90 °C. Five of these substrates were loaded with gold (Au): two with polymer-encapsulated gold (Au_L4 and Au_L12, corresponding to a “thin” and a “thick” insulating layer, respectively) and three with PANI-encapsulated gold (Au_PANI30, Au_PANI90, and Au_PANI180, corresponding to a “thin”, “thick”, and “very thick” conductive layer, respectively). Equal metal loadings (0.015 mg) on the substrates were verified by quantified Spectroquant measurements. The reference substrate that contained the pristine TiO2 was loaded with equal volume of water to adapt for the potential enhancement effect of surface hydroxylation. All of the substrates were dried at 90 °C for 6 h. The substrates were then spin-coated with 100 µL of a 0.15 wt % stearic acid solution in chloroform and dried at 80 °C for 15 min. The designations of the different Au-TiO2 plasmonic systems are listed in Table 1 for ease of understanding. Additional details regarding the photocatalytic reactor setup and measurements are provided in the Supporting Information.

Acknowledgments

This work was supported by Research Foundation Flanders (FWO). P.C. and R-G.C. acknowledge financial support from FWO (Project No. G038215N). N.C. and S.B. acknowledge financial support from the European Research Council (ERC Starting Grant No. 335078-COLOURATOM).